# ABSTRACT

Neutrinos are one of the most interesting particles in the Standard Model (SM). They are the second most abundant particle in the universe after photons. Their elusive nature, owing to their neutral charge and interaction exclusively through the weak force, makes the study of neutrinos exceptionally difficult. The discovery of neutrino oscillations by both Super-Kamiokande [1] and Sudbury Neutrino Observatory [2] has shed new light on exploring new physics beyond the SM (BSM). Neutrino oscillations essentially validate that neutrinos possess mass and provide an initial concrete experimental hint of BSM physics. The parameters linked with neutrino oscillations are extensively being investigated in various neutrino experiments [3–6]. Neutrinos serve as a promising pathway to delve into new physics within the leptonic sector. The BSM models, often come with some new additional unknown interactions of neutrinos termed non-standard interactions (NSIs). Given the precision of current and future neutrino experiments, these subdominant effects of neutrinos can significantly impact the physics potential of various neutrino experiments.

The non standard couplings of neutrinos with a vector is a well-explored area of neutrino physics. Apart from that neutrinos may also couple with a scalar to produce rich phenomenology in different neutrino experiments [7]. Recently, there has been an exploration of potential unconventional interactions between neutrinos and a scalar field [7–10]. This scalar interaction appears as a correction to the neutrino mass term [11], which can yield interesting phenomenological outcomes distinct from those arising from the vector-mediated NSIs. Numerous investigations have been conducted to assess the impact of these scalar NSI (SNSI) elements, considering astrophysical, cosmological, terrestrial, and space-based experimental constraints [11]. Also, the inclusion of scalar NSI has been employed to account for observed Borexino data [7]. These scalar couplings might also influence the measurement of various neutrino oscillation parameters across different neutrino experiments. Also, the effects of scalar NSI directly scale with the environmental matter density, making long-baseline neutrino experiments well-suited for probing its effects.

**Objectives:** The objectives of the thesis are listed as follows,

- To study the theoretical and phenomenological signatures of scalar non standard interactions in both neutrino oscillations & interactions and development of a framework to probe its effects in neutrino oscillation probabilities.

- To explore the possible impact of scalar non standard effects on the sensitivities of the neutrino experiments, primarily long baseline neutrino experiments and perform a synergy analysis combining different long baseline experiments.

- To simulate detector response for neutrino experiments viz. Hyper Kamiokande and associated detector instrumentation.

The objectives of the work have been divided into two goals. In the first two objectives, we have performed the study of scalar NSI in neutrino oscillations and explored the sensitivity of various detectors to such effects. In the third objective, we have performed a simulation study for the detector response in various experiments and probe-associated instrumentation.

❑ **Exploration of scalar NSI:** We investigate both the theoretical and phenomenological manifestations of scalar NSI in both neutrino oscillations and interactions and formulate a framework for probing these effects in the probabilities of neutrinos. Additionally, we aim to assess the potential influence of its effects on the sensitivities (CP measurements, neutrino mass measurement) of neutrino experiments, primarily focusing on Long Baseline (LBL) experiments. Finally, we conduct a synergy analysis by integrating data from different LBL experiments to gain comprehensive insights into the impact of scalar NSI parameters.

❍ **Formalism of scalar NSI:** The inclusion of non-standard effects into the theory directly alters the neutrino interaction Lagrangian, subsequently modifying the neutrino Hamiltonian in matter. This modified Hamiltonian, incorporating the new non-standard interaction, allows for the exploration of oscillation probabilities. The effective Lagrangian for neutrino-matter interactions can be framed as [12],

$$\mathcal{L}_{\rm cc}^{\rm eff} = -\frac{4G_F}{\sqrt{2}} \left[\overline{\nu_e}(p_3)\gamma_\mu P_L \nu_e(p_2)\right] \left[\overline{e}(p_1)\gamma^\mu P_L e(p_4)\right], \tag{1}$$

where, $P_L$ and $P_R$ denote left and right chiral projection operators, with $P_L = (1-\gamma_5)/2$ and $P_R = (1+\gamma_5)/2$ and $G_F$ is the Fermi constant. The effective Hamiltonian ($\mathcal{H}_{\rm matter}$) governing neutrino oscillations in matter can be expressed as [13],

$$\mathcal{H}_{matter} \approx E_\nu + \frac{MM^\dagger}{2E_\nu} \pm V_{\rm SI}\,, \tag{2}$$

where, $E_\nu$ represents the neutrino energy, M stands for the neutrino mass matrix, and $V_{\rm SI}$ denotes the neutrino matter potential and the positive or negative sign of before the '$V_{SI}$' term is for neutrino or antineutrino modes respectively. The effective Lagrangian describing neutrinos coupled through a scalar can be expressed as [7, 11],

$$\mathcal{L}_{\rm eff}^{\rm S} = \frac{y_f y_{\alpha\beta}}{m_\phi^2}(\bar{\nu}_\alpha(p_3)\nu_\beta(p_2))(\bar{f}(p_1)f(p_4))\,, \tag{3}$$

where, $\alpha$ and $\beta$ denote the neutrino flavors, while $f$ represents matter fermions, $y_{\alpha\beta}$ signifies the Yukawa couplings between neutrinos and the scalar mediator $\phi$, $y_f$ represents the Yukawa coupling of $\phi$ with matter fermions $f$, and $m_\phi$ is the mass of the scalar mediator. The effective Hamiltonian [11, 14, 15], incorporating scalar NSI effects, can be expressed as follows:

$$\mathcal{H}_{\text{SNSI}} \approx E_\nu + \frac{M_{\text{eff}} M_{\text{eff}}^\dagger}{2E_\nu} \pm V_{\text{SI}}\,, \tag{4}$$

where, $M_{\text{eff}}$ represents the effective mass matrix, encompassing both the conventional mass matrix $M$ and the SNSI contribution, $\delta M \equiv \sum_f n_f y_f y_{\alpha\beta}/m_\phi^2$ and may be written as, $M_{\text{eff}} = M + \delta M$. We define the SNSI mass correction term $\delta M$ as,

$$\delta M \equiv \sqrt{|\Delta m^2_{31}|} \begin{pmatrix} \eta_{ee} & \eta_{e\mu} & \eta_{e\tau} \\ \eta_{\mu e} & \eta_{\mu\mu} & \eta_{\mu\tau} \\ \eta_{\tau e} & \eta_{\tau\mu} & \eta_{\tau\tau} \end{pmatrix} . \tag{5}$$

❍ **Neutrino oscillation probabilities in presence of scalar NSI:** We note that the modified Hamiltonian in presence of NSI will introduce changes to the oscillation probabilities. To assess the impact of NSI, we first probe its effects on the probabilities [1]. In figure 4.1, we show the effects of the diagonal scalar NSI element $\eta_{ee}$ on $P_{\mu e}$ as a function of neutrino energy for various baselines corresponding to DUNE (left), T2HK (middle) and T2HKK (right). The inclusion of scalar NSI parameters induces notable effects on the oscillation probabilities at all three baselines, particularly near the points of oscillation maxima. A positive (negative) $\eta_{ee}$ amplifies (suppresses) the probabilities near the oscillation maxima. The visible effects of scalar NSI on neutrino oscillations are interesting and we explore it further by constructing a statistical $\chi^2$ framework to probe it in detector sensitivities.

❍ **Effects on CP measurement sensitivity:** In figure 3.7, we show the CP-precision measurement capability of DUNE in presence of diagonal scalar NSI elements $\eta_{ee}$, $\eta_{\mu\mu}$, and $\eta_{\tau\tau}$. The analysis signifies, knowing the true values of $\delta_{CP}$, how precisely it can constrain the test $\delta_{CP}$ values. It may be observed that the capability of DUNE in constraining the $\delta_{CP}$ phase gets enhanced (worsened) for positive (negative) values of $\eta_{ee}$. For the 'no scalar NSI' case (the red curve), DUNE should be able to measure $\delta_{CP}$ with a precision of $\sim$ -90$^{\circ}{}^{+45^\circ}_{-48^\circ}$ at $3\sigma$ CL.

❍ **Synergy of various LBL experiments:** We discuss here the effects of $\eta_{\alpha\beta}$ on the CPV sensitivities at DUNE, T2HK and T2HKK. The CPV sensitivity is calculated

[1] NuOscProbExact [16] package is used for this analysis

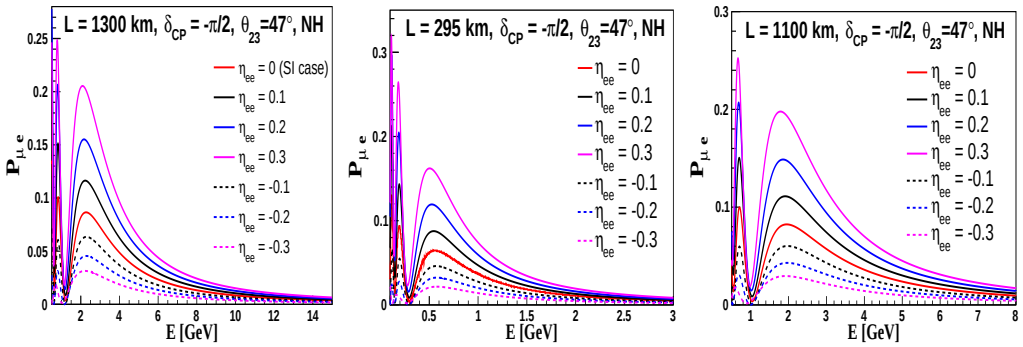


FIGURE 1: The effects of $\eta_{ee}$ on $P_{\mu e}$ at the baselines of DUNE (left), T2HK (middle) and T2HKK (right) for $\delta_{CP}$ = -$\pi/2$, $\theta_{23} = 47^\circ$ and NH. The red solid–curve is for no–NSI case while other solid (dashed) curves are for positive (negative) NSI parameters.

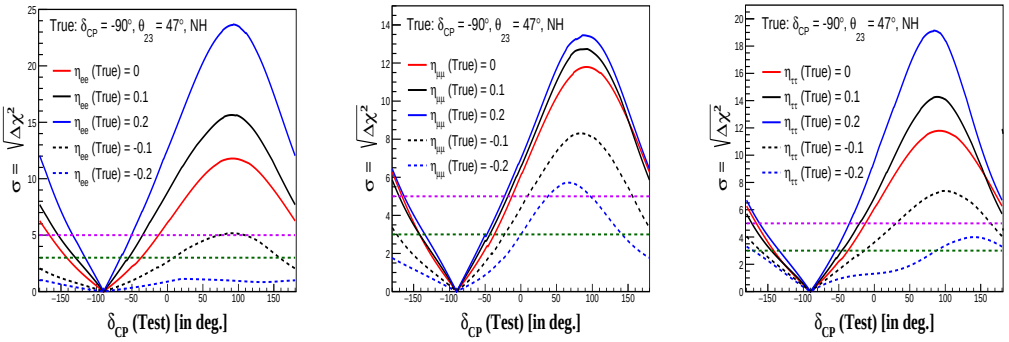


FIGURE 2: The CP-precision sensitivity of DUNE in presence SNSI at true $\delta_{CP}$=-$\pi/2$, $\theta_{23}$=47° for $\eta_{ee}$(top-left panel), $\eta_{\mu\mu}$(top-right panel) and $\eta_{\tau\tau}$(bottom panel) [8].

as,

$$\Delta\chi^2_{\rm CPV}\ (\delta^{\rm true}_{\rm CP}) = \min\ \left[\chi^2\ (\delta^{\rm true}_{CP}, \delta^{\rm test}_{CP} = 0),\ \chi^2(\delta^{\rm true}_{CP}, \delta^{\rm test}_{CP} = \pm\pi)\right]. \qquad (6)$$

In figure 4.7, we show the effects of scalar NSI on the CPV sensitivity by combining data from all three experiments. We see that, the experiment's sensitivity towards CPV gets significantly affected by the inclusion of scalar NSI. The combined study improves the sensitivities including the overlapped region particularly due to the collection of data in a broader range of degenerate spaces. It may be noted that, for a positive (negative) $\eta_{\alpha\beta}$, an analysis combining all the three experiments shows a significant improvement (deterioration) in CPV sensitivities.

❍ **Neutrino mass measurement:** The presence of scalar NSI can bring a direct dependence of absolute neutrino masses via neutrino oscillations. In this work, for the first time, we obtain a bound on the lightest neutrino mass by probing neutrino oscillation experiments. In figure 5.5, we show the allowed region for $1\sigma$, $2\sigma$ and $3\sigma$ CL in $\eta_{\alpha\beta} - m$ planes for DUNE considering NH of neutrinos. The lightest neutrino mass can be constrained as $m_1 \in [0.009, 0.03]$ eV at $1\sigma$ CL for $\eta_{ee}$. The element $\eta_{\mu\mu}$ can constrain the neutrino mass as $m_1 \in [0.016, 0.024]$ eV at $1\sigma$ CL. For $\eta_{\tau\tau}$, we see a similar constrain on $m_1 \in [0.017, 0.023]$ eV at $1\sigma$ CL.

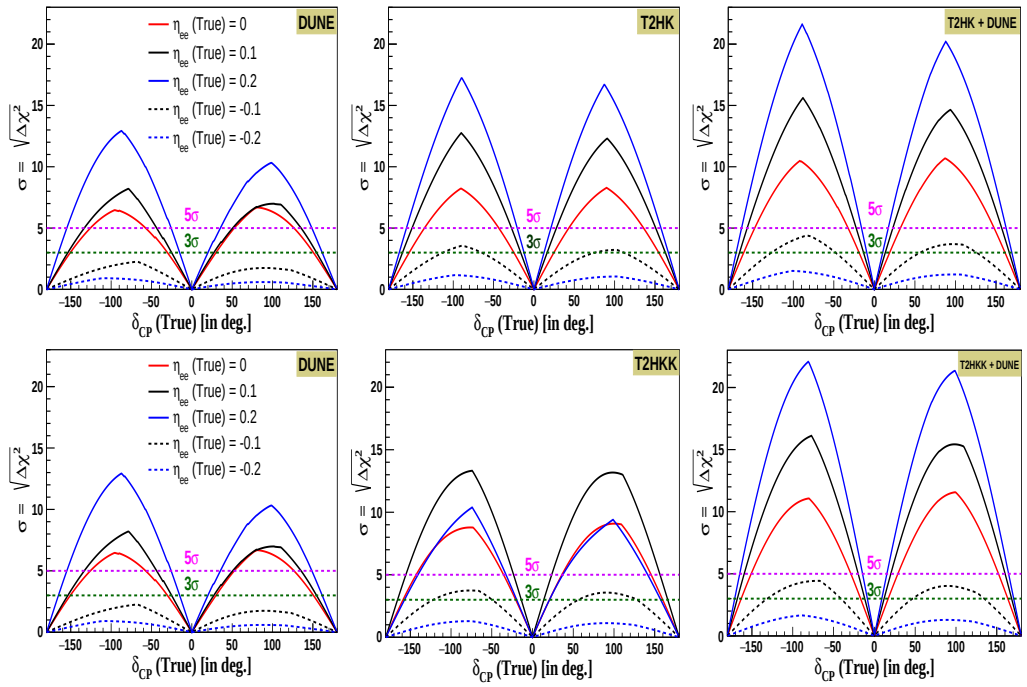


FIGURE 3: The CPV sensitivity of *Top:* DUNE (left–column), T2HK (middle-column) and DUNE + T2HK (right-column), *Bottom:* DUNE (left–column), T2HKK (middle-column) and DUNE + T2HKK (right-column) in presence of scalar NSI parameter $\eta_{ee}$. The solid-red curve is for the no scalar NSI case whereas solid (dashed) black and blue curves are for positive (negative) $\eta_{\tau\tau}$ [9].

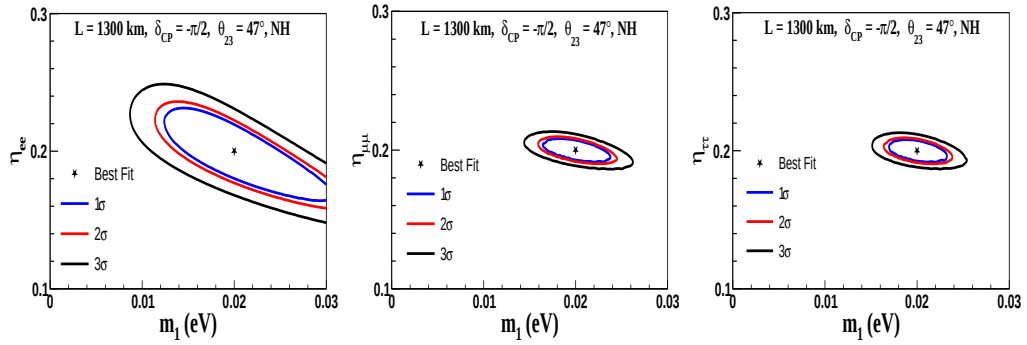


FIGURE 4: Allowed region of lightest neutrino mass for normal hierarchy for the diagonal NSI parameters $\eta_{ee}$ (left-panel), $\eta_{\mu\mu}$ (middle-panel) and $\eta_{\tau\tau}$ (right-panel). The blue, red and magenta lines represent the $1\sigma$, $2\sigma$ and $3\sigma$ confidence level. The best fit values of $(\eta_{\alpha\beta}, m)$ are $(0.2, 0.02eV)$ and $(0.2, 0.015eV)$ for NH and IH respectively [10].

❑ **Detector Simulation & Instrumentation work:** This section outlines a comprehensive framework for our endeavors in detector simulation and instrumentation work. We also highlight our interesting results in the following subsections.

❍ **Simulation of gamma-ray background at HK:** For the detector simulation

work, we have considered primarily the proposed Hyper Kamiokande (HK) detector in Japan. For simulation studies, GEANT4[2] package is extensively used and the package used by the HK collaboration is WCSim[3]. The presence of gamma-ray background radiation has the potential to exert an influence on the sensitivity of the Hyper Kamiokande detector at lower energies. All the details of the abundance of the isotopes as well as the energy spectrum associated with these isotopes have been provided by the HK collaboration. In this work, we have analyzed the gamma-ray spectrum associated with this background radiation. We have integrated both abundance and energy spectrum information to provide a comprehensive representation of the gamma background. The ratio of the input and output energy histogram is performed after scaling the input histogram,

$$R = \frac{Output\ Energy\ Spectrum}{Input\ Energy\ Spectrum}$$

We have performed the study with varying numbers of events as shown in the figure 5. We note that, as the number of statistical data points increases, the ratio tends towards unity, signifying improved concordance between our simulation results and the input data information.

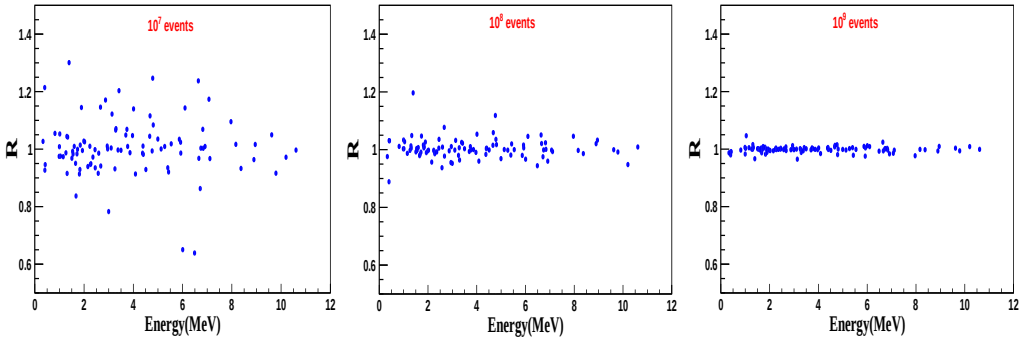


FIGURE 5: Ratio of isotope energy spectrum as a function of input energy for different statistics.

❍ **Probing neutrino mass ordering using HK supernova simulation** For the exploration of supernova neutrinos at HK, we employ the SNOwGLoBES [4] package for simulating the experiment. We show in figure 6, the comparison of different SN models (Garching) for HK [17] and JUNO [18]. The red (blue) colour points are for NH (IH) for different Garching supernova mass models. We see that the events are well separable for both NH and IH for various supernova models. However, the discrimination is poor in JUNO due to the large uncertainties. This is because the number of events detected by JUNO is quite smaller compared to those of HK.

[2]https://geant4.web.cern.ch
[3]https://github.com/WCSim/WCSim
[4]https://github.com/SNOwGLoBES/snowglobes

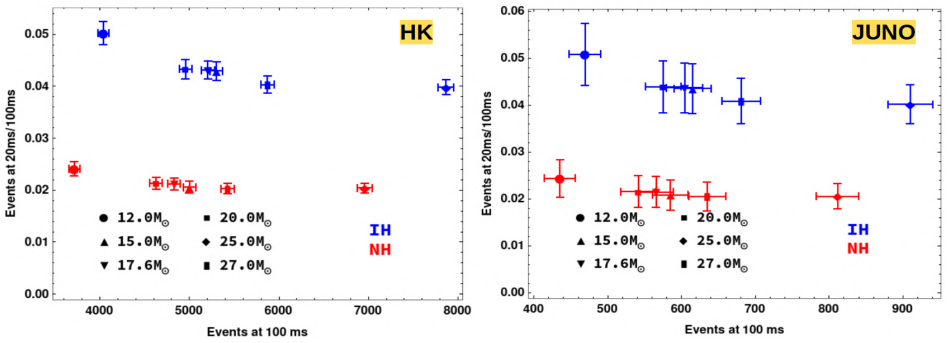


FIGURE 6: Event ratio plot for different supernova mass models (Garching) for both NH and IH for HK (left) and JUNO (right). Red (blue) colour is for NH (IH) with varied progenitor masses.

❍ **Detector Instrumentation: Leak test of RPC** In terms of instrumentation, our focus has primarily been on evaluating the Resistive Plate Chamber (RPC) detector and assessing its efficiency for potential use in experiments. We primarily worked on the fabrication and subsequent testing of RPC. To ensure an experiment's success, each RPC must operate without displaying notable signs of aging throughout its entire operational duration. So, it is important to conduct a thorough leak test on RPC glass gaps both during production and throughout operation for the successful operation of an experiment. The RPC gap was tested for approximately 23 hours. The value of the leak constant $C_{Leak}$ calculated from the analysis is:

$$C_{Leak} = -(6.698) \times 10^{-3}\,\mathrm{ml\,hour^{-1}\,mmWC^{-1}}.$$

In this context, a negative $C_{Leak}$ value signifies an inward leak, indicating that a

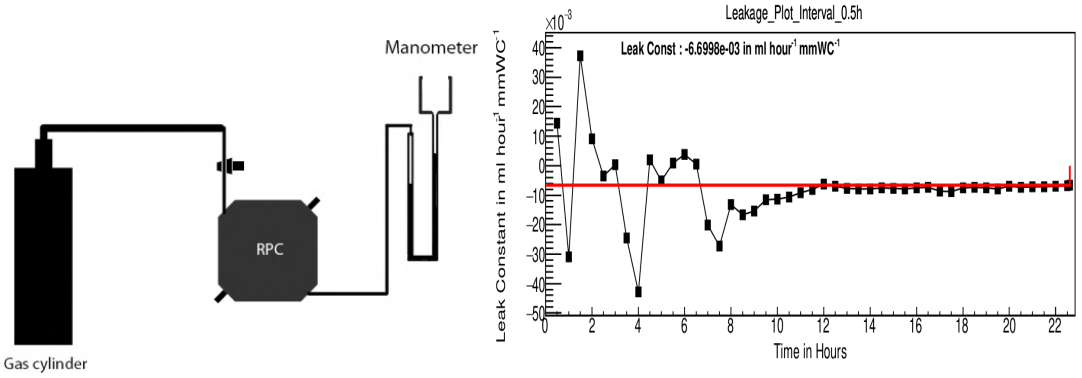


FIGURE 7: *Left:* Schematics of a typical leak test setup; *Right:* Leak rate of RPC as a function of time.

constant pressure difference of 40 mmWC between the inside and outside of an RPC gap will result in a leakage of 6.43 ml of gas over 24 hours. The small magnitude of $C_{Leak}$ suggests that this gap has a relatively minor leak. To determine the optimal or minimum duration required for a reliable leak rate calculation, the data was

divided into various sets covering different time durations from the test's start time, and the $C_{Leak}$ value was computed. In Figure 6.18, the $C_{Leak}$ value for the varying time at an interval of 30 minutes is presented. For the RPC gap, it becomes evident that a minimum of 11-12 hours is necessary to estimate the leakage accurately.

❑ **Organization of the thesis:** In alignment with the defined objectives, the thesis has been structured into seven chapters. We present a concise overview of the chapters in our thesis using the following flowchart 2.3.

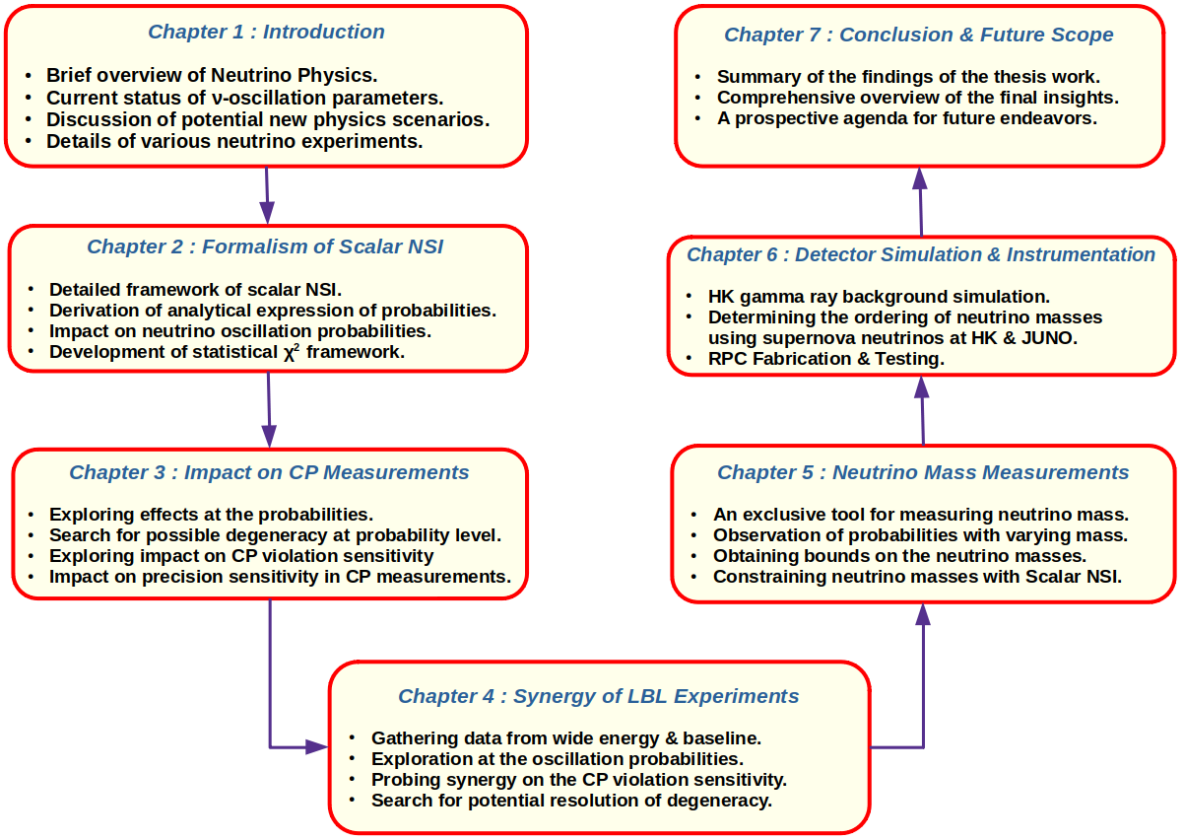


FIGURE 8: A flowchart depicting the structure of the thesis.

**Keywords:** Neutrino Physics, Non Standard Interactions, Beyond Standard Model, CP Violation, Neutrino Mass, Long Baseline Experiments.